Two-colour infrared missile warning sensors

Filip Neele*
TNO Defence, Security and Safety, The Hague, The Netherlands

ABSTRACT

Current missile-warning sensors on aircraft mostly operate in the ultraviolet wavelength band. Aimed primarily at detecting short-range, shoulder-fired surface-to-air missiles, the detection range of the sensors is of the same order as the threat range, which is 3-5 km. However, this range is only attained against older missiles, with bright exhaust flames. Modern missile developments include the use of new propellants, which generate low-intensity plumes. These threats are detected at much shorter ranges by current ultraviolet warning sensors, resulting in short reaction times. Infrared sensors are able to detect targets at a much longer range. In contrast with the ultraviolet band, in which a target is observed against an almost zero background, infrared sensors must extract targets from a complex background. This leads to a much higher false-alarm rate, which has thus far prevented the deployment of infrared sensors in a missile warning system. One way of reducing false-alarms levels is to make use of the spectral difference between missile plumes and the background. By carefully choosing two wavelength bands, the contrast between missile plume and background can be maximised. This paper presents a method to search for the best possible combination of two bands in the mid-wave infrared, that leads to the longest detection ranges and that works for a wide range of missile propellants. Detection ranges predicted in the infrared will be compared with those obtained in the ultraviolet, to demonstrate the increased range and, therefore, the increased reaction time for the aircraft.

Keywords: missile warning, infrared signature, exhaust plumes, propellants

1. INTRODUCTION

Missile warning sensors that are currently in use operate in the ultraviolet part of the spectrum. At these wavelengths, a low to almost zero background enables the use of simple detection algorithms and the near absence of both natural and man-made sources that emit ultraviolet radiation results in a low false alarm rate. The latter is a primary requirement for a fully automatic self-protection system. The disadvantage of the use of ultraviolet is that the atmosphere strongly absorbs the ultraviolet radiation, limiting the detection ranges of typical threat missiles to a few kilometres[1,2]. Whereas this provides sufficient warning time for the older missiles with bright exhaust plumes, the detection range for modern stealth propellants can become insufficient for the deployment of countermeasures[2]. Warning sensors operating in the infrared domain are generally seen as the future successors of current systems, as at infrared wavelengths the threat can be detected from longer ranges. However, the need for image processing to detect the target in the complex infrared scene and to obtain a sufficiently low false alarm level have so far prevented the development of successful systems. Infrared warning sensor development is in essence an optimisation problem with many variables. In many studies, a two- or multi-filter approach is used[3], to exploit the spectral differences between targets and backgrounds. Some authors approach the problem from the sensor side, to develop a technically feasible sensor[3,4]. This paper approaches the problem from a theoretical point of view, with the aim to define a method that finds the best set of two filters, that maximises detection range and that minimises false alarm rate. Technical aspects of sensor system design are not addressed in this paper.

The following sections outline the method used to obtain the best choice of two filter bands in the 3-5 µm band. Typical missile plumes are computed for both high-intensity and stealth propellants. This provides not only a realistic range of threat signatures in terms not only of total intensity, but also of spectral behaviour. Detection ranges are computed for a hypothetical sensor operating in background-limited mode, which provides an upper limit to sensor performance. It is shown that the design of infrared threat warning sensors is relatively insensitive to the spectral nature of the threat

* filip.neele@tno.nl; phone +31 70 374 0461; fax +31 70 374 0654

Airborne Intelligence, Surveillance, Reconnaissance (ISR) Systems and Applications II,
edited by Stephan H. Wyatt, Proceedings of SPIE Vol. 5787 (SPIE, Bellingham, WA, 2005)
0277-786X/05/$15 · doi: 10.1117/12.603391

signature. The detection of targets that could generate false alarms, such as warm or hot objects and sun glint, is modelled and the suppression by a two-colour infrared system is shown.

2. METHOD

2.1 Targets: missile plume spectral emission

Generally, the infrared signature of a missile is dominated by the emission from its exhaust plume. The hardbody signature dominates only at near nose-on aspect angles, when most of the plume is hidden behind the missile body. The infrared signature of the hardbody is assumed to be due to aerodynamic heating and is derived from the relation $T = T_{air}(1+0.176M^2)$, where T is the missile body temperature, T_{air} is the ambient air temperature and M is the Mach number (see, e.g., ref. [5]). The emissivity of the missile coating is 0.8.

The code NIRATAM[6] is used to compute the spectral emission from the missile plume. Table 1 lists the exit plane conditions for the four propellants that were used in the current study. The propellants range from high-thrust aluminised fuel (HTPB-AP-Al) to low-intensity fuels (HTPB-AP, GAP/AN). The exit radii listed in the table were adjusted to result in equal thrust for the four propellant types, which makes it possible to directly compare results for the different propellants. Flow fields for different missile speeds were computed with the REP code[7,8], which were used as input to NIRATAM to produce aspect-angle dependent emission spectra in the 3-5 µm band.

Table 1. Parameters for plume structure and composition modelling[9]. Nozzle radius is adjusted for each propellant to achieve the a thrust of 1kN for all propellants. Table reproduced from ref. [2]. Missile velocity is 500 m/s.

	HTPB-AP-Al	HTPB-AP	GAP/AN	Kerosene
Exit radius [mm]	16.2	16.3	23.2	13.71
Axial velocity [m/s]	2404.6	2388.1	2292.4	2688
Radial velocity [m/s]	356.7	354.2	340.0	
Exit pressure [kPa]	200.4	168.7	57.6	1
Exit temperature [K]	2327.2	1578.0	689.4	1745.5
Exit plane mole fractions				
N2	8.151×10^{-2}	9.912×10^{-2}	2.517×10^{-1}	2.120×10^{-1}
CO	2.106×10^{-1}	6.745×10^{-2}	1.344×10^{-1}	2.306×10^{-1}
H2O	1.368×10^{-1}	4.212×10^{-1}	3.943×10^{-1}	2.812×10^{-1}
CO2	1.713×10^{-2}	1.537×10^{-1}	7.773×10^{-2}	1.681×10^{-1}
H2	2.985×10^{-1}	6.370×10^{-2}	1.390×10^{-1}	1.081×10^{-1}
H	4.094×10^{-3}	8.000×10^{-6}	1.090×10^{-4}	7.155×10^{-5}
OH	3.210×10^{-4}	2.000×10^{-6}	3.800×10^{-5}	1.099×10^{-5}
O2	1.000×10^{-6}	1.000×10^{-8}	1.000×10^{-8}	6.493×10^{-9}
O	3.000×10^{-6}	1.030×10^{-8}	1.000×10^{-8}	5.593×10^{-9}
HO2	1.000×10^{-8}	1.000×10^{-8}	1.000×10^{-8}	1.000×10^{-15}
Cl	1.552×10^{-3}	2.000×10^{-5}		
Cl2	1.000×10^{-6}	1.000×10^{-8}		
HCl	1.576×10^{-1}	1.929×10^{-1}		
Al2O3	9.065×10^{-2}			
MgO			2.661×10^{-3}	

Plume spectra are shown in Figures 5 through 8 (left panels in figures). Figure 5 shows the spectrum, at 5° off nose, for the aluminised, high-intensity HTPB-AP-Al fuel; the non-aluminised HTPB-AP plume spectrum is shown in Figure 6. Both plume were computed for a missile speed of 500 m/s. As the thrust of the all propellants listed in Table 1 is equal, the results in Figure 5 through 8 correspond to missiles with the same performance. The aluminium that is added to the HTPB-AP-Al propellant to increase the thrust increases the MWIR signature by a factor of at about ten in the 3-5 µm band. The contribution from the target body, although it is at a temperature of over 120 °C, is insignificant in the wavelength band shown. The missile body is 2 m long and 8 cm in diameter. Figure 7 shows the spectrum for a plume of a missile with GAP/AN propellant. This propellant burns at a relatively low temperature and produces a plume that is a factor of about five lower in intensity than from the non-aluminised HTPB-AP propellant. This propellant may be

indicative of future low-intensity propellants. A spectrum for a kerosene plume is shown in Figure 8. This spectral emission from this plume differs from that of the other three (solid) propellants, which results in different optimum filter bands for an infrared warning sensor, as shown in the following sections.

2.2 Atmosphere

A look-up table of spectral atmospheric transmission was computed with MODTRAN[10], for the standard mid-latitude summer atmosphere, over a horizontal path of variable length. Transmission for a specific path length was computed through interpolation of the look-up table. The aerosol type was set to rural, with a visibility of 14 km. The contrast of the target (missile) at the sensor was found by multiplying the zero-range spectral emission with the transmission spectrum for a given path length, adding the path radiance (assuming an air temperature of 15 °C) and integrating over the sensor waveband. This is explained in more detail in section 2.5. Figure 1 shows the transmission over a horizontal path with a length of 2 km, in the 2-6 µm band. The CO_2 absorption band around 4.3 µm is already clearly defined. The interval 3.4-4.0 µm is characterised by relatively high transmission.

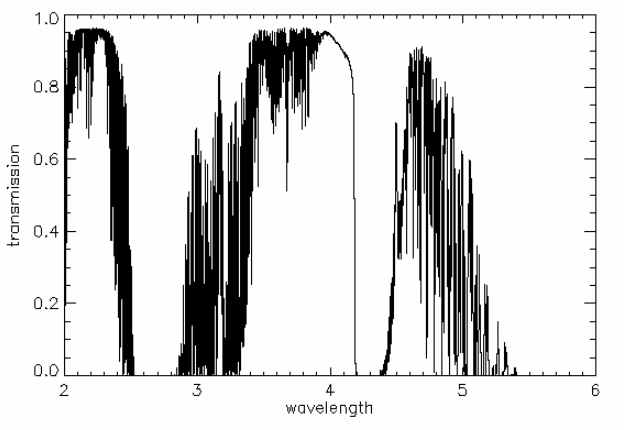

Figure 1. Spectral transmission in the 2-6 µm range, over a horizontal path of 2 km. The atmosphere is the MODTRAN[8] standard atmosphere mid-latitude summer.

2.3 Backgrounds, sun glint

The background, against which the target is observed, is assumed to be at a fixed temperature. Noise is represented by small variations in the apparent temperature of the background. Figure 2 shows two background spectra, corresponding to apparent temperatures of 15 °C and 15.5 °C. This clutter level is relatively low for land backgrounds, but has the proper magnitude for (overcast) sky backgrounds. Land backgrounds, which are relevant to the study of missile warning sensor performance for the case of surface-to-air missile detection, are complex and are not considered explicitly here. Elements in the background are treated in section 3.2. Sky backgrounds are relevant for air-to-air scenarios and for ground-to-air scenarios in which the airborne platform is at a higher altitude. The noise in the background was computed from the curves in Figure 2, for the appropriate sensor waveband. The temperature variations were assumed to occur on a spatial scale equal to the sensor instantaneous field of view.

The right-hand-side panel in Figure 2 shows a spectrum of a sun glint, which is considered in the following sections as a possible source of false alarm. The sun glint was computed by assuming a horizontal surface of 5×5 m², with an infrared reflectivity of 5%, representative of standard coatings, and a BRDF lobe width of 3°. As evident from the two panels in the figure, the sun glint is several orders of magnitude more intense than the background, with the intensity decreasing towards longer wavelengths, in contrast with the spectral behaviour of the background.

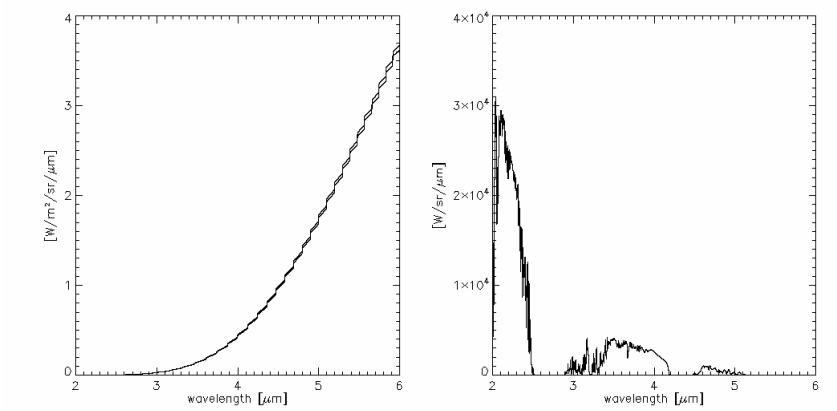

Figure 2. Left: background spectra, for apparent background temperatures of 15 °C and 15.5 °C. Right: spectrum of sun glint off a 5×5 m² object.

2.4 Sensor

The sensor is assumed to be background-limited and to operate in photon-counting mode. The irradiance on the detector, in terms of photons per frame is computed with the expression

$$N_v = \int \xi(\lambda) L(\lambda) d\lambda \tag{1}$$

where λ is wavelength (μm), L is pixel (ir)radiance and ξ a parameter that converts radiance to photon count (in units of photons per pixel per frame) on a single detector element. The integration in (1) is over the sensor wavelength band. The parameter ξ is given by

$$\xi(\lambda) = \frac{\pi D^2 A_d \lambda t_{\text{int}}}{4 l^2 h c} \tag{2}$$

where D is the lens diameter, A_d the area of a single detector element, t_{int} the integration time, l the focal length, h Planck's constant and c the speed of light. For the current study, D=5 cm and A_d=20×20 μm. The focal length l can be varied to obtain different values for the instantaneous field of view (IFOV), although for this paper only a single IFOV is considered.

To find those combinations of two bands within the interval 3-5 μm that yield the best detection of missile plumes, a search through sensor parameter space is conducted. The sensor parameter space is defined by IFOV, waveband centre and waveband width. The pixel field of view (IFOV) is defined to be 0.5 mrad; the band centre is varied from 3 to 5 μm with steps of 0.08 mrad and the band width is varied from 0.01 μm to 1.5 μm in steps of 0.06 μm.

Current missile warning sensors operating in the ultraviolet, where no background signal is present, have a typical spatial resolution of 1° (about 17 mrad). For the IR sensors a higher spatial resolution is needed to detect the weak signal from a distant target in the strong background signal. Note that pixel size is less significant for current (ultraviolet) sensors, due to the absence of background radiation. For sensors operating in the (solar blind) ultraviolet, pixel size only affects the angular resolution.

2.5 Detection range

For each hypothetical sensor, defined by IFOV, λ_c and $\Delta\lambda$, target contrast is computed at a series of ranges (1, 2, 4, 6, 10, 15, 20, 25, 30, 35, 40 and 100 km). At each range the irradiance on a pixel containing the target is computed with

(3) $$E_{TGT} = \frac{\tau_{atm} A_{TGT} L_{TGT}}{R^2} + \alpha \Omega L_{bkg} + \frac{A_{TGT}}{R^2} L_{path} \text{ W/m}^2$$

where τ_{atm} is atmospheric transmission, L_{TGT} target radiance [W/m²/sr], A_{TGT} target area [m²], L_{BKG} background radiance [W/m²/sr], Ω the pixel solid angle and R the range to the target. The second term in (3) represents the contribution from the background, when the target does not completely fill the pixel (the factor α is the fill factor). The last term in (3) gives the radiance of the atmosphere along the optical path to the sensor. Although not explicitly indicated in (3), at each range a check is performed of whether the target fills a pixel. Path radiance and the contribution from the background are added to the total irradiance accordingly. Pixel irradiance is converted to photon flux using the expressions given in section 2.5, giving photon flux N_{TGT} for the target pixel and N_{BKG} for a pixel on the background.

In the computation of (3), the approximation is made that the radiance of the background is given by the ambient air temperature. Expression (3) is computed as an integration over the sensor waveband, to account for the spectral character of transmission and target and background radiance.

Using these expressions, target irradiance contrast is computed as a function of range. For all combinations of two wavebands, the ratios r_{TGT} and r_{BKG} are computed:

(4) $$r_{TGT}(R) = \frac{N_{TGT,1}(R)}{N_{TGT,2}(R)}, \quad r_{BKG} = \frac{N_{BKG,1}}{N_{BKG,2}}$$

At each range, the contrast of the target ratio in the two filters with the background ratio is computed. Detection is assumed to take place once the ratio exceeds the detection threshold:

(5) $$\frac{r_{TGT} - r_{BKG}}{\sigma_{BKG}} \geq k\, SNR_{threshold}$$

where σ_{BKG} is the noise level in the background and k is a parameter that can be tuned to control the false alarm rate. The noise level in the background ratio follows from both the noise level in the background for each of the filter bands and apparent temperature variations in the background (clutter). For a background-limited sensor, the former is given by the square root of the photon flux in each of the two filter bands. The clutter in the background is derived from the background spectra given in Figure 2 and added to the intrinsic background noise. The threshold for detection, k, should follow from an analysis of possible targets and structures in the background.

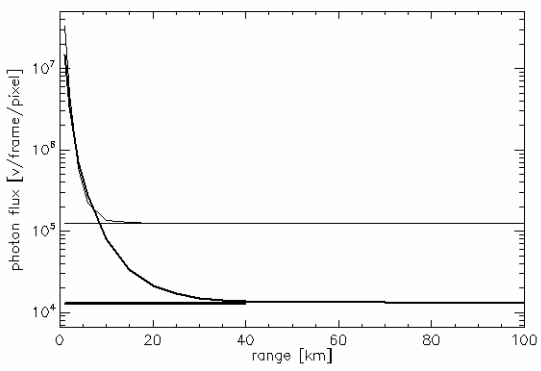

Figure 3. Irradiance (of the pixel containing the target) in terms of photon flux per pixel per frame as a function of target range for a missile with the HTPB-AP-Al propellant. The sensor is assumed to be in photon-counting mode (background limited). The horizontal lines in the diagram represents the flux from the background (at 15 °C). The sensor pixel size is 0.5 mrad. Thin curve: wavelength band 4.49 – 4.56 µm; thick curve: 3.45 – 3.52 µm.

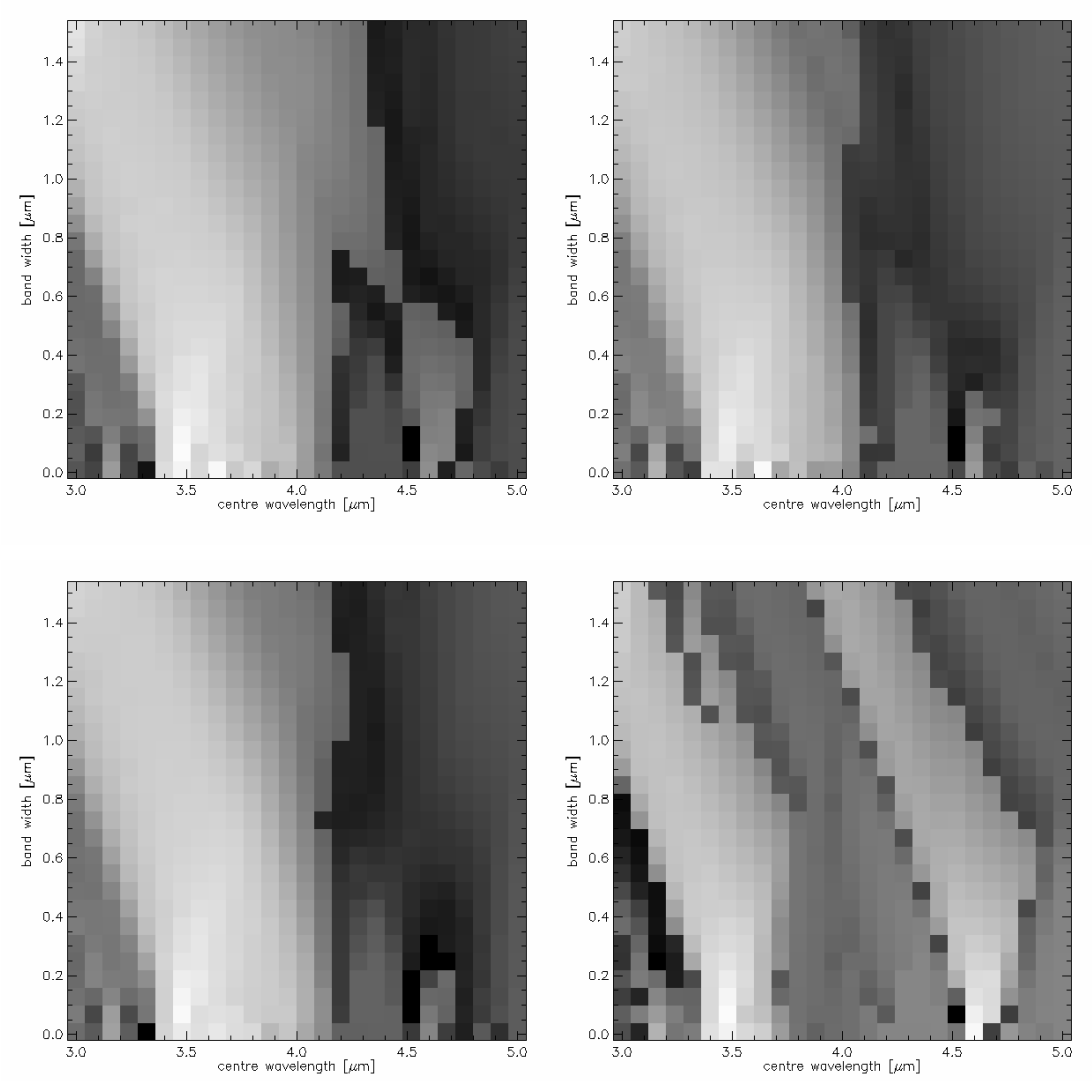

Figure 4. Plots showing detection range as a function of centre wavelength (horizontal axis) and bandwidth (vertical axis) of the second filter. The first filter is 4.49 – 4.56 µm. Top left: HTPB-AP-Al propellant; the colour scale runs from zero (black) to 28.5 km (white). Top right: the same, now for propellant HTPB-AP (maximum range in panel is 14.5 km). Bottom left: propellant GAP (maximum range in panel is 10.5 km). Bottom right: kerosene plume (maximum range in the panel is 28.5 km).

Figure 3 shows two examples of photon count from a missile plume as a function of range, for two filter bands. The vertical axis in the figure gives photon flux (in units of photons/frame/pixel). The horizontal lines in the panels represent the irradiance from the background. In the two wavelength bands shown, the target can be detected to ranges of about 30 km (in the 4.49 – 4.56 µm band) and 12 km (in the band 3.45 – 3.52 µm). It can be expected that when the data from the two bands are combined to compute the spectral ratio that the detection range is smaller than 30 km. However, the goal behind the development of two-colour systems (or multi-band systems) is not to optimise detection range, but to minimise false alarms. This is discussed further in the following sections.

3. RESULTS

3.1 Missile targets

Using the propellants listed above, all possible filter combinations in the 3-5 µm band, with the limitations in filter location and width as given above, were considered. This results in a 4-dimensional data base of detection ranges. For clarity, results are shown below for a single choice of the first filter, showing the dependence of sensor performance (=detection range) on the choice of the second filter.

Detection range as a function of centre wavelength and bandwidth of the second filter, with a fixed first filter, is shown in Figure 4, for the propellants HTPB-AP-Al (aluminised, top left panel) and HTPB-AP (non-aluminised, top right panel). The detection threshold used was k=5. Results for the low-intensity GAP propellant are shown in the bottom left panel in Figure 4, while results for a (hypothetical) missile with kerosene are shown in the bottom right panel. The diagrams show detection range for all possible combinations of centre wavelength (restricted to the MWIR band) and bandwidths between 0.01 and 1.5 µm. The first filter is 4.49 – 4.56 µm, in the red wing of the CO_2 radiance of the target plume. This filter gives almost the maximum detection ranges for all propellants. It is noted that the colour scales are different for the four panels in the figure. The panels show that when one of the filter is chosen so as to sample the red wing of the CO_2 radiance, the best performance of the MWS is obtained for only a few narrow-band filters near 3.5 µm. Figure 1 shows that this is the short-wavelength edge of the interval of high transmissions extending to about 4 µm. Combined with the decreasing radiance of the plumes with increasing wavelength in that same interval, this explains the optimum location of the second filter. The plume spectra in Figures 4 through 7 show that the spectral ratio between the red wing and a narrow band near 3.5 µm interval produces large contrasts with the spectral ratio in the background (shown in Figure 2).

This is illustrated in Figure 5 (left panel), which shows the HTPB-AP-Al plume spectrum, with the two filters superimposed that represent the maximum detection range in the top left panel in Figure 4. Where the left panel in Figure 5 shows the intrinsic plume spectrum, the right-hand-side panel in the figure shows irradiance as a function of range. Spectra at ranges from 1 to 35 km are shown. The decrease in spectral energy in the 3.5 – 4.2 µm is relatively independent of wavelength, which is the origin of the broad range of filter possibilities that give a good sensor performance (see Figure 4 and Figure 1).

A similar spectral behaviour with increasing range is shown in Figures 6 and 7, for the HTPB-AP and GAP propellants, although the spectral intensity of the signal is much lower than for the aluminised HTPB-AP-Al propellant. The results in Figure 4 also show that the choice of wavebands is insensitive to threat type. With the exception of the kerosene plume, sensor performance is maximum for the same set of two filters. The intrinsic spectrum and range-dependent

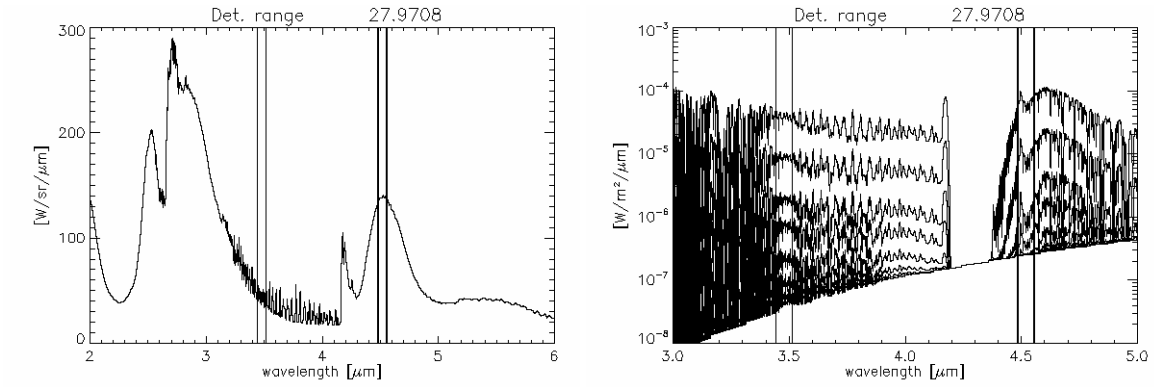

Figure 5. HTPB-AP-Al plume spectrum, with superimposed filter bands 4.49 – 4.56 µm (the filter used in the computation of the results shown in Figure 4) and 3.45 – 3.52 µm, which is the combination of filters resulting in maximum detection range in the top left panel in Figure 4. The right-hand-side panel shows plume spectra as a function of range, to illustrate the wavelength and range dependence of atmospheric transmission (ranges of 1 to 35 km, top to bottom).

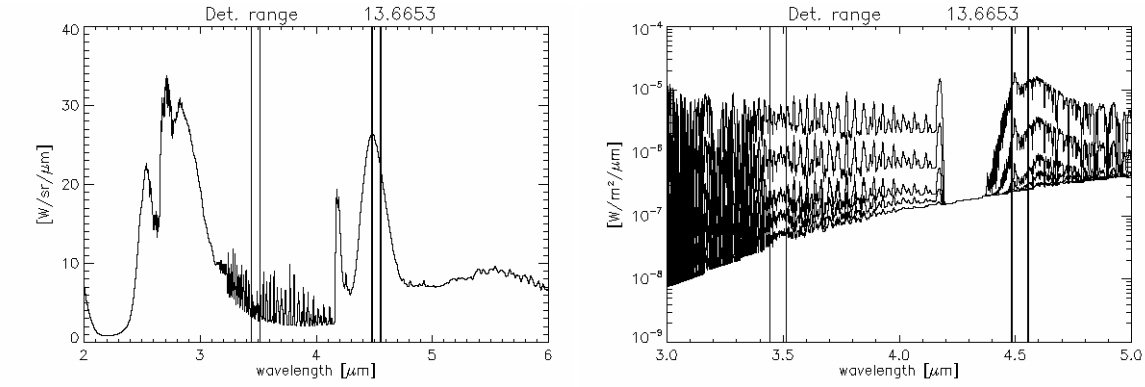

Figure 6. As Figure 5, now for a HTPB-AP (non-aluminised) plume, with superimposed filter bands 4.49 – 4.56 μm (the filter used in the computation of the results shown in Figure 4) and 3.45 – 3.52 μm.

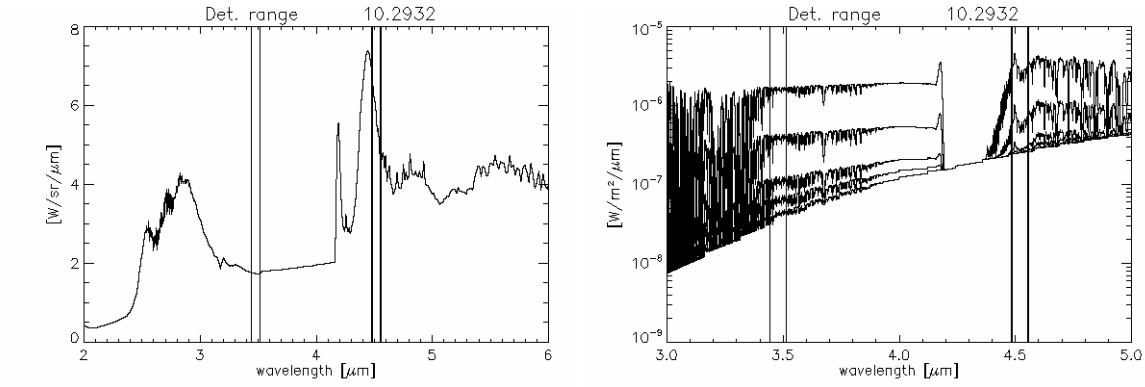

Figure 7. As Figure 5, now for a GAP plume, with superimposed filter bands 4.49 – 4.56 μm (the filter used in the computation of the results shown in Figure 4) and 3.45 – 3.52 μm.

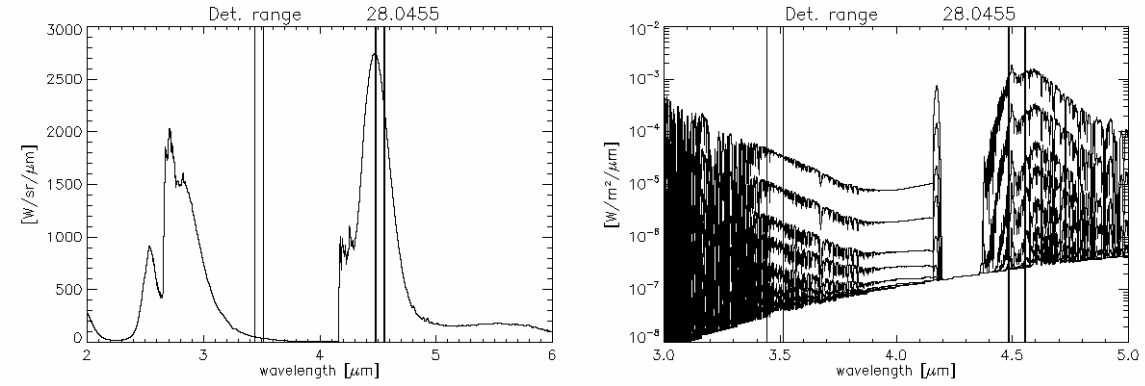

Figure 8. As Figure 5, now for a kerosene plume, with superimposed the same filter bands as in the previous figures.

irradiance for the kerosene plume is shown in Figure 8. The optimum filter choice for kerosene plumes are plotted in the figure. The filters differ from those found for the other plumes, but sample the same general wavelength bands. This feature could provide the means to discriminate between aircraft plumes (including afterburner plumes) and missile plumes.

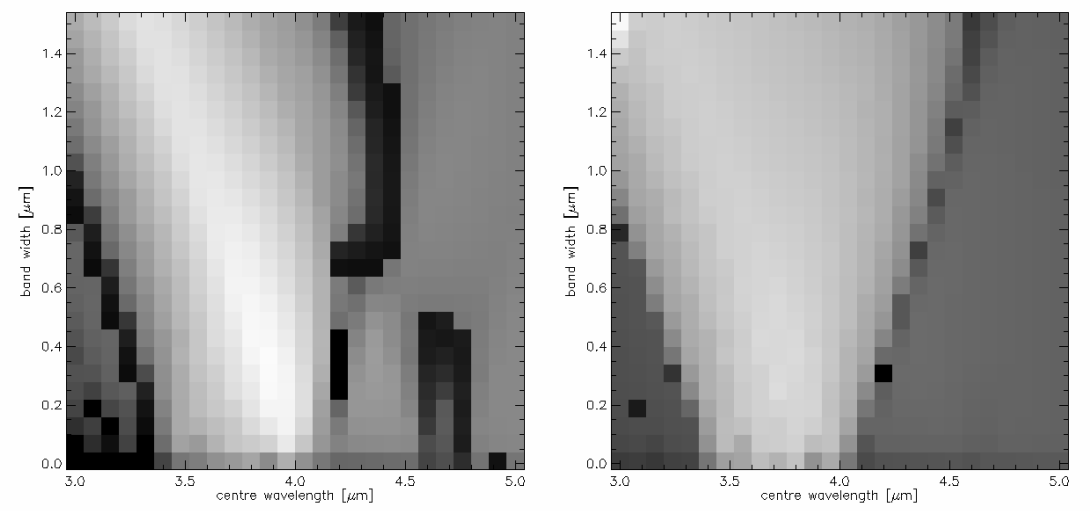

Figure 9. Left: blackbody at 45 °C (maximum range in the panel is 25.1 km). Right: sun glint on a horizontal surface (maximum range in panel is 118 km). In both cases the first filter is 4.49 – 4.56 µm, the same as that used for the filter diagrams in Figure 4.

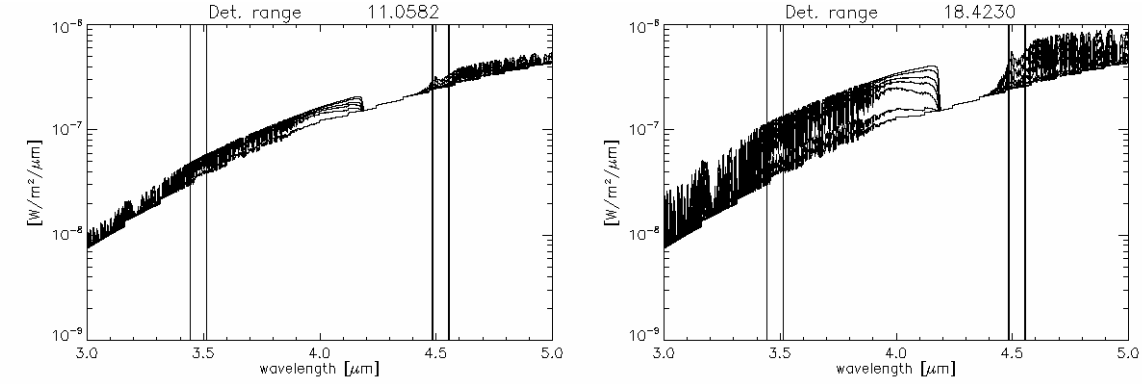

Figure 10. Blackbody target spectra as a function of range, for the filter combination 4.49 – 4.56 µm and 3.45 – 3.52 µm, as in the previous figures. Left: 25 °C blackbody; right: 45 °C blackbody. The detection range is relatively large due to the spectral ratio between the two filter bands, caused by atmospheric absorption, rather than by inherent spectral differences between target and background. Note that irradiation levels are (much) lower than for missile targets or sun glint.

3.2 False alarms

The signal-to-noise threshold for detection used in Figure 4 through 8 was 5, more or less a standard value for the detection of point sources. However, the rationale for the development of a two-colour warning sensor is to reduce the false alarm rate to an acceptable level, while retaining the possibly long detection ranges at infrared wavelengths. The SNR threshold for detection should be based on an analysis of detection ranges of objects in the infrared scene that could give rise to false alarms.

Figure 9 (left panel) shows a filter diagram, similar to those in Figure 4, for a blackbody target at 45 °C. The first filter is the same as those in Figure 4 through 8. The similarity is noted of the filter diagrams to those obtained for the missile targets (Figure 4). Range-dependent irradiance, for the same set of filters as used in Figure 4 through 8, is shown in Figure 10, for blackbody targets at 25 °C (left panel) and 45 °C (right panel). In spite of the fact that their intrinsic spectra are similar to that of the background (which is at 15 °C), the spectral ratio for these targets is not close to zero. Due to atmospheric absorption, the spectral ratio of the target in the two filter bands is large enough to result in an

appreciable detection range. This is clearly illustrated in Figure 10. It is noted that the spectral ratio increases with range, due to stronger absorption in the filter 4.49 – 4.56 µm. The irradiation levels, however, are lower than those from the missile targets. Therefore, filter choice based on the spectral character of missile targets does not automatically lead to rejection of warm or hot elements in the infrared scene as targets. The combination of spectral ratio and signal strength might be an additional discriminative for the rejection of these objects as false targets.

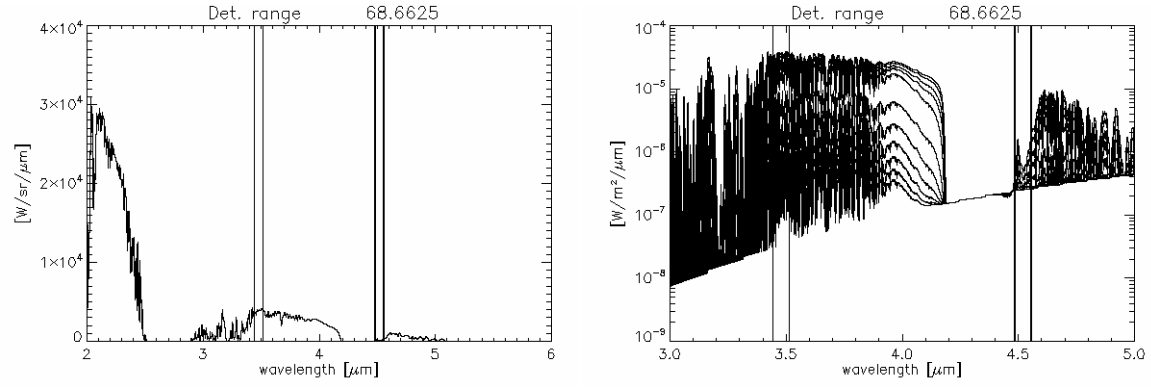

Figure 11. As Figure 5, now for a sun glint (see Figure 2), with superimposed filter bands 4.49 – 4.56 µm (the filter used in the computation of the results shown in Figures 4 and 9) and 3.45 – 3.52 µm.

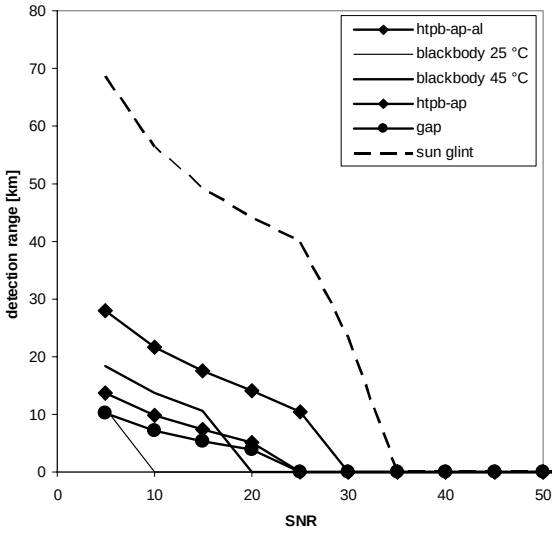

Figure 12. Detection range as a function of SNR detection threshold for several missile plumes and two objects with a blackbody temperature of 25 °C and 45 °C. Also shown is a curve for sun glint (see also Figure 2). Filters used are the same as in the previous figures.

The right panel in Figure 9 shows a filter diagram for a sun glint off a horizontal target, as described in section 2.3. Range-dependent spectra for sun glint are shown in Figure 11. The detection range (69 km in this case) is determined by the size of the target (5×5 m²), rather than by atmospheric transmission or signal strength. The spectra shown in the figure show signal strength and illustrate that the spectral ratio that decreases only slowly with increasing range. These results indicate that additional measures must be taken to prevent false alarms from sun glint.

3.3 False-alarm reduction

Figure 12 shows the detection range as a function of detection threshold for three missile propellants used above and two blackbodies. Increasing the SNR threshold to above 10 will remove from the scene seen by the sensor any objects with a blackbody temperature below 25 °C (and temperature contrast below 10 °C). At the same time, the detection range of missiles with HTPB-AP-Al propellant is decreased by about 20%, relative to the case for a detection threshold of SNR=5, to about 22 km (for the atmospheric conditions used here). A further increase in the detection threshold to 20 will remove from the scene all objects with a blackbody temperature below 45 °C (temperature contrast below 30 °C). This will probably result in a low false alarm level, as it is fair to assume that few natural objects have a temperature higher than 30 °C with the average background, at the cost of an significantly decreased detection range of missile plumes. For this detection threshold, the high-intensity aluminised plumes can be observed to distances of about 15 km, but the propellants that produce low-intensity plumes can now be observed only at distances shorter than about 5 km.

Figure 12 also shows a detection curve for sun glint. The glint, for which the spectrum is shown in Figure 2, has a high spectral ratio and can be observed at long range. An elevated detection threshold does not remove glint from the list of possible false alarms. As has been noted previously[4], an additional feature of sun glint, at least when it occurs on large surfaces such as lakes, is that the glint appears stationary in a sensor's field of view. As a result, an analysis of the relative motion in the scene can not be used to dismiss glint as a false alarm. The results presented here show that a two-colour system not necessarily automatically suppresses glint. The same is true when one of the filter bands is chosen to sample the blue spike of the CO_2 plume radiance.

3.4 Comparison with ultraviolet band

In a previous paper[2], the detection range of the same plumes was analysed for the ultraviolet wavelength band. The detection ranges found, for similar atmospheric conditions, varied from more than 8 km for the HTPB-AP-Al plume to less than 0.5 km for the non-aluminised HTPB-AP plumes. Where the high-intensity plumes are detected at long range, leaving sufficient time for countermeasures, the low-intensity and stealth threats are detected only at the last moment. Clearly, a sensor operating at infrared wavelengths provides a much longer warning time. Even when the detection threshold is increased to suppress warm and hot targets in the infrared scene, the detection range of missile plumes is such that sufficient warning time is left, even for the low-intensity plumes. The additional warning time can be used for additional analysis of the target signal, such as relative motion in the field of view of the sensor(s) and signal growth, to further decrease false alarm rate.

4. DISCUSSION

The analysis presented here shows that two-colour infrared systems can be used in a missile warning role, to improve over the limited detection ranges provided by the current systems operating at ultraviolet wavelengths. A method is presented to search for those combinations of two filters in the 3-5 µm band that produce the best sensor performance (longest detection ranges) against current missiles. Several propellant types are analysed, ranging from high-intensity aluminised propellants to low-intensity fuels representative of (future) stealth missiles. One of the main drawbacks of infrared systems is the presence of background radiance, which results in higher false alarm levels than in the ultraviolet band. The analysis shown here proves that in a two-colour system the false alarm rate can be reduced by increasing the detection threshold in the spectral ratio of the two filter bands. It is evident that this also reduces the detection range of the threat, yet the detection ranges remain significantly longer than at ultraviolet wavelengths. This results in sufficient warning time for the deployment of countermeasures. One element of the infrared scene that may be difficult to suppress is sun glint.

The results presented here are a first step towards a full optimisation process to find the best choice of two (or more) filter bands in the mid-wave infrared region for a missile warning sensor. Several elements of the multi-parameter optimisation process have been addressed, such as threat signatures (different propellant types), atmospheric effects (transmission losses) and sources of false alarm (objects in the infrared scene, sun glint). The first results indicate that a robust infrared system is feasible, with the offer of detection ranges (and warning times) that are much longer than those possible with current ultraviolet systems.

5. ACKNOWLEDGEMENTS

This work has been done under contracts from the Royal Netherlands Air Force.

REFERENCES

1. Neele, F.P. and H.M.A. Schleijpen, *UV missile plume signatures*, in: Targets and backgrounds VIII: characterisation and representation, Proc. SPIE, vol. 4718: p. 369-379, SPIE, Orlando, 2002.
2. Neele, F.P. and H.M.A. Schleijpen, *Electro-optical missile plume detection*, in: Targets and backgrounds IX: characterisation and representation, Proc. SPIE, vol. 5075, p. 270 – 280, 2003.
3. R. Breiter, W. Cabanski, K.-H., Mauk, W. Rode, J.Ziegler, H, Schneider and M. Walter, *Multicolor and dual-band IR camera for missile warning and automatic target recognition*, in: Targets and backgrounds VIII: characterisation and representation, Proc. SPIE, vol. 4718: p. 280-288, SPIE, Orlando, 2002.
4. B. Molocher, A. Kaltenecker and M. Assel, *MCIR-MWIS: results from test campaigns*, paper presented at the 6th Joint Internat. Milit. Sensing Symp., Dresden, 2004.
5. R.D. Hudson, *Infrared system engineering*, Wiley, New York, 1969.
6. M. Fair, NATO IR Air Target Signature Prediction Model (NIRATAM), 2nd NATO IRIS Joint Symposium June 1996.
7. J.M. Cousins, *Calculation of conditions in an axi-symmetric rocket exhaust plume: the REP3 computer program*, DERA technical report 218, Westcott, United Kingdom, 1982.
8. D.A.B. Fuggle, D.P. Hills, A. Christopher and H. Mace, *An efficient procedure for solving the chemical species transport equations in the computer program REP3*, DERA technical report 262, Westcott, United Kingdom, 1983.
9. J. Rapanotti, B. Gilbert, G. Richer and R. Stowe, *IR sensor design insight from missile plume prediction models*, in: Targets and Backgrounds VIII: characterisation and representation, W.R. Watkins, D. Clement and W.R. Reynolds (eds.), Proc. SPIE, vol. 4718, p. 289-298, 2002.
10. MODTRAN Air Force Research Laboratory web site: http://www.vs.afrl.af.mil/Division/VSBYB/modtran4.html.